ROYAL SOCIETY
OF CHEMISTRY

PAPER

Insights into the nucleophilic substitution of pyridine at an unsaturated carbon center†

Pan Du,‡[a] Jiyang Zhao, [ID] ‡*[b] Shanshan Liu[b] and Zhen Yue[b]

Bimolecular nucleophilic substitution (S_N2) is a fundamental reaction that has been widely studied. So far, the nucleophiles are mainly anionic species in S_N2 reactions. In this study, we use density functional theory calculations to assess the mechanisms of substitution of carbonyl, imidoyl, and vinyl compounds with a neutral nucleophile, pyridine. Charge decomposition analysis is performed to explore the main components of the transition state's LUMO. For reactions of imidoyl or carbonyl compounds with pyridine or Cl^-, the LUMOs of the transition states are composed of mixed orbitals originating from the nucleophile and the substrate. Considering the unique mixed nature of the orbitals, the reaction mode is termed S_Nm (m means mix). Moreover, the main components of the transition state's LUMO are pure σ^*_{C-Cl} MO in the reactions of $H_2C{=}CHCl$ with pyridine or Cl^-. Computations were also performed for $RY{=}CHX$ substrates with different X and Y groups (X= Cl^-, Br^-, or F^-; Y = O, N, or C).

Introduction

Bimolecular nucleophilic substitution (S_N2) is a fundamental reaction that is implicated in different chemical and biological processes.[1–10] This reaction is triggered by the attack of a nucleophile (Nu^-) on a central atom (A), which results in the displacement of a leaving group (Y) (Scheme 1(a)). The nucleophilic attack can occur from the backside (S_N2-b) or front side (S_N2-f) of the reacting molecule. For most compounds, S_N2-b is preferred to S_N2-f, and the central atom at which substitution occurs is sp^3 hybridized. However, in some cases, nucleophilic substitution may occur at sp^2 hybridized olefinic sites, and the reaction is referred to as nucleophilic vinylic substitution (S_NV) (Scheme 1(b)).[11–14] S_NV reactions proceed via perpendicular concerted π attack with retention ($S_NV\pi$) or via in-plane σ^* attack with inversion ($S_NV\sigma$).

Although the mechanisms of nucleophilic substitution are well established for many substrates, the exact reactions steps for imidoyl and carbonyl compounds are controversial.[15–21] According to Bach and Lee, the nucleophilic substitution of these compounds proceeds via the out-of-plane $S_NV\pi$ mechanism (Scheme 1(b)).[15,16] However, Lee and Yamabe show that X^-

+ RCOY displacement reactions cannot follow the $S_NV\pi$ mechanism since the σ^*_{C-Y} molecular orbital (MO) is the main component of the transition state's LUMO, and since the $\pi^*_{C=X}$ and σ^*_{C-Y} MOs are efficiently mixed.[17–21]

The nucleophiles involved in S_N2 and S_NV reactions are mainly anionic species, such as Cl^-, Br^-, I^-, OH^-, CN^-, and SH^-. Neutral nucleophiles are very rare, particularly the large ones.[22,23] Recently, we had studied the electrophilic addition reactions of pyridine to acyl chlorides, chloroformates and chloro-oxime reagents (Scheme 2).[24,25] These reactions can be described as S_N2 reactions, where pyridine, a bulky neutral compound, is the nucleophile, and Cl^- is the leaving group. Considering that pyridine and anionic species (ex. Cl^-) exhibit significantly different electrostatic potential diagrams (Fig. 1), it is expected that their nucleophilic activity and mechanism will also be different. In this study, we investigate the S_N2 reactions of pyridine with three kinds of substrates (RCOCl, RClCNR and RClCCR₂, shown in Scheme 2).

Computational details

Quantum chemistry calculations were conducted by the Gaussian16 program.[26] The geometries of all stable species and transition states were optimized using the M06-2X functional with 6-311+G(d,p) basis set.[27–30] All calculations were conducted in dichloromethane solution using the self-consistent reaction field (SCRF) method with the IEFPCM solvation model.[31] The harmonic frequencies were calculated at the same level of theory in order to obtain the relevant thermodynamic energy corrections and to characterize the optimized stationary points as minima or saddle points. To ascertain the reasonability of our computational method, other functionals (QCISD, MP2, PBE1PBE, B3LYP, B3LYP-d3, w-b97xd) were also used to

[a]*School of Life Science and Chemistry, Jiangsu Second Normal University, Nanjing, 210013, China*

[b]*School of Environmental Science, Nanjing Xiaozhuang University, Nanjing, 211171, China. E-mail: jyzhao1981@163.com*

† Electronic supplementary information (ESI) available: The transition states and mixing orbitals of the carbonyl and imidoyl substrates, the profile scans of nucleophile (pyridine or Cl^-) approach to substrates, corrected free energies, imaginary frequency and Cartesian coordinates are included in the ESI. See DOI: 10.1039/d1ra03019a

‡ P. Du and J. Zhao contributed equally to this work.
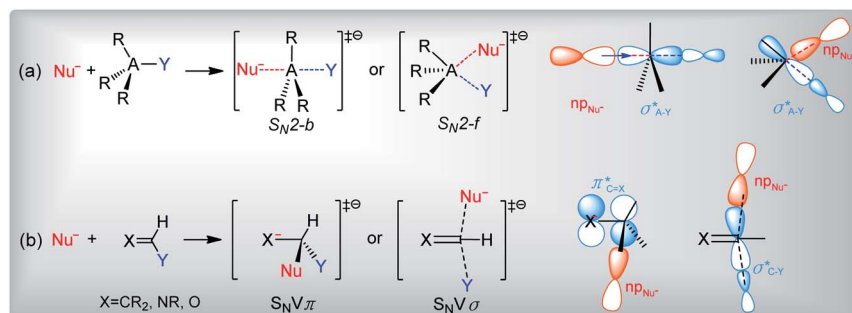
Scheme 1 General reaction schemes and molecular orbital interactions of (a) S_N2 and (b) S_NV reactions. Nu^- is the nucleophile, A is the central atom, and Y is the leaving group.
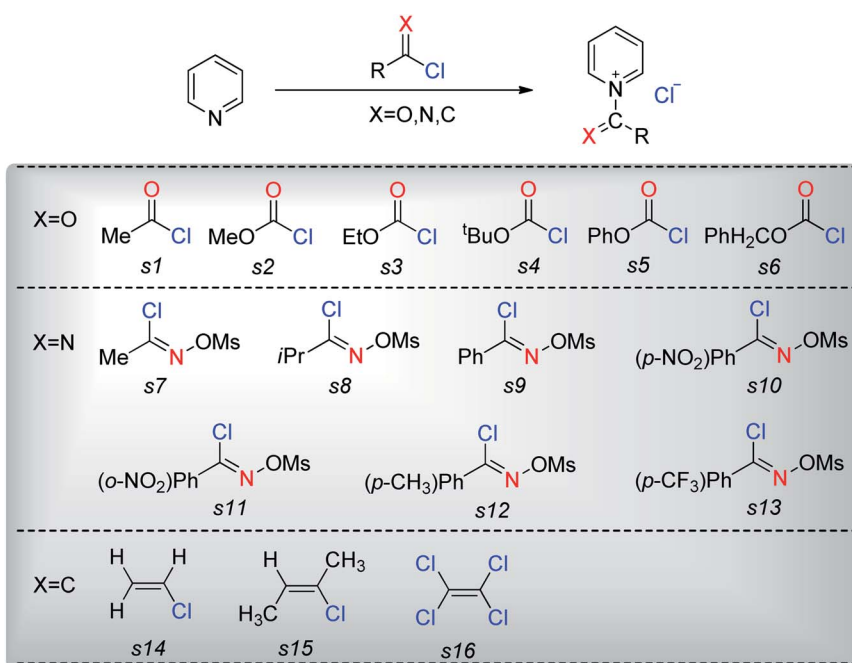
Scheme 2 Electrophilic addition of pyridine to RCOCl, RClCNR and RClCCR$_2$.

investigate the structures and energies of some important intermediates and transition states. The Gibbs free energies of all species were determined at $T = 298.15$ K and $P = 1$ atm. Intrinsic reaction coordinate (IRC) analysis was used to confirm important transition states and natural bond orbital analyses

Fig. 1 Electrostatic potential diagrams of pyridine and Cl^- (isosurface = 0.05 a.u.). Red and blue regions in the ESP map represent areas of negative and positive potential, respectively.

were carried out at the M062x/6-311+G** level.[32–36] The 3D-optimized structures in this study were observed using the CYLview visualization program.[37] As for the orbital interactions and orbital composition analysis, they were studied according to the charge decomposition analysis (CDA) method and Hirshfeld method implemented in the Multiwfn program.[38–46] IBO (intrinsic bond orbital) analyses was performed to study the electronic structure changes in the reaction of pyridine with CH_3COCl along the reaction pathway.[47]
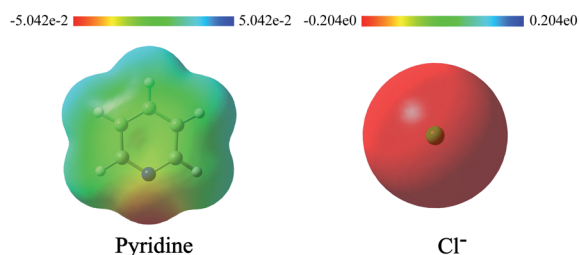
Results and discussion

1 Nucleophilic substitution reactions of CH_3COCl with pyridine or Cl^-

The nucleophilic substitution reactions of acyl chloride CH_3-$COCl$ with pyridine or Cl^- are shown in Fig. 2. Considering that pyridine is not charged, it shows no minima related to the reactant complex, unlike the anionic nucleophile. However, the
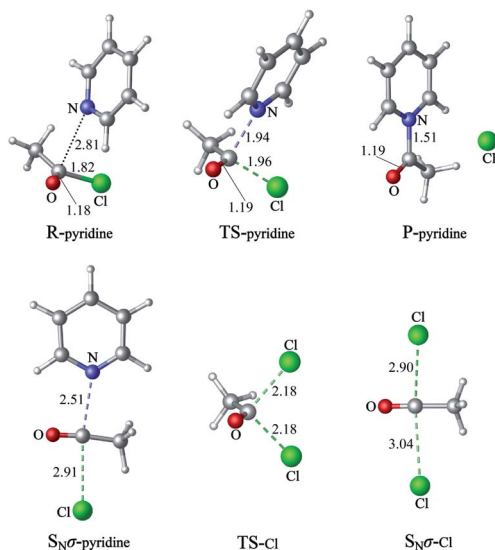
Fig. 2 The nucleophilic substitution reactions of acyl chloride CH_3-$COCl$ with pyridine or Cl^- (R: reactant, TS: transition state, P: product).

Fig. 3 IBOs of the two reactive orbitals in the reaction of pyridine with CH_3COCl along the reaction pathway.

Cl^- eliminated by the nucleophilic attack of pyridine leads to a potential well that is associated with product complex. The transition state (TS$_{-pyridine}$, illustrated in Fig. 2) shows that when pyridine attacking the substrate, it induces the formation of a C–N bond and the simultaneous cleavage of the C–Cl bond. Fig. 3 shows that the IBOs transform continuously from the electronic structure of the starting material to that of the product along the intrinsic reaction coordinate. Two IBOs show a concerted transformation of one pyridine lone pair (top) into a Cl–C σ bond, while the C–Cl σ bond (down) breaks and transforms into a lone pair. Based on the calculated energy values, the free energy barrier of the reaction is only 13.8 kcal mol^{-1} (in dichloromethane), which indicates that pyridine is a strong nucleophile. The distance between the carbon center on acyl chloride and the nitrogen atom of pyridine is shortened from 2.81 Å in the reactants to 1.94 Å in the transition state, and to 1.51 Å in the product complex. Meanwhile, the C–Cl bond is elongated from 1.82 Å in CH_3COCl to 1.96 Å in the transition state. Using the ωb97xd and B3LYP-*d3* functionals, the related reaction barriers are 13.0 and 15.5 kcal mol^{-1}, respectively, indicating that the results obtained using the two functionals and M062X functional are in good agreement. The structures of the transition states calculated by ωb97xd and B3LYP-*d3* functionals are shown in Fig. S1 in the ESI.†

Although the reaction of nucleophilic substitution of acyl chloride with Cl^- has been studied extensively, we chose to investigate it as well for the purpose of direct comparison.[15–21] As shown in Fig. 2, the transition state in this reaction (TS$_{-Cl}$) is characterized by a C–Cl bond length of 2.18 Å, which is longer than that calculated for TS$_{-pyridine}$. Also, the dihedral angle Cl–O–C–C in TS$_{-pyridine}$ (139.4°) is greater than that in TS$_{-Cl}$ (126.9°), which suggests that Cl^- induces more deformation of acyl chloride than pyridine due to its more negative charge and less hindrance.
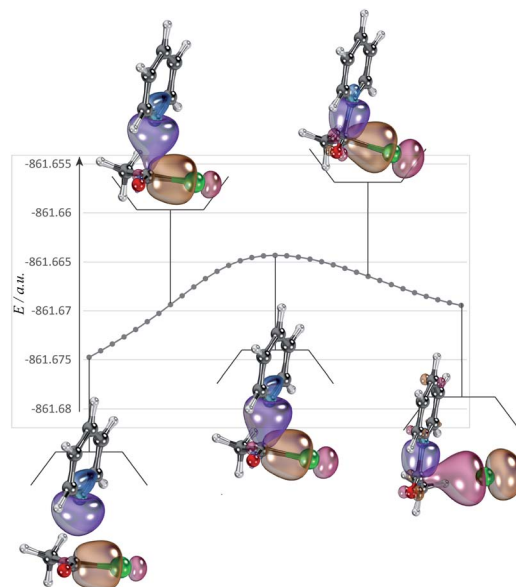
When pyridine approaches the central carbon of CH_3COCl, an electron migrates from the electron-rich HOMO of the nucleophile to the LUMO of the substrate, which result in the deformation of the latter.[17,18] Considering that the energy gap between the π*$_{C=O}$ and σ*$_{C–Cl}$ molecular orbitals of CH_3COCl is small (1.3 eV), electron migration from pyridine induces sufficient mixing of these two MOs.[15,17–19,21] Based on the results of charge decomposition analysis (CDA)[38–42] illustrated in Fig. 4, the LUMO (orbital 44) of the reactant complex (Int 1) is primarily composed of acyl chloride's orbital 21 (π*$_{C=O}$, LUMO). However, as pyridine approaches, orbitals 21 and 24 of pyridine gradually mix into the LUMO of the complex (orbital 44), along with orbital 21 of CH_3COCl. In the transition state, the LUMO is formed by mixing the orbitals 21 and 24 of pyridine with orbitals 21 and 22 of CH_3COCl. Based on the orbital composition analysis (Fig. 3(TS)), atom orbitals of chloride and carbonyl oxygen have 17.3% and 8.3% contributions to MO 44 in the transition state, respectively, indicating that the σ*$_{C–Cl}$ MO becomes the main component of the transition state's LUMO. Therefore, it may be concluded that the nucleophilic substitution reaction is initiated by the attack of pyridine's np orbital on the π*$_{C=O}$ MO of CH_3COCl. Knowing that after charge transfer, σ*$_{C–Cl}$ is mixed into the LUMO of CH_3COCl, eventually it becomes the major component. Considering the transition state's LUMO is a mixed orbital, the attack mode is labeled **SNm** (m means mix).

CDA was also performed on the reaction of Cl^- and CH_3COCl. The results shown in Fig. 5 demonstrate that the transition state's LUMO consists of orbital 7 (np) of Cl^- and orbitals 21 and 22 of CH_3COCl. The contributions of chloride atom orbital and carbonyl oxygen atom orbital to MO 30 in the transition state are 12.8% and 12.7%, respectively, indicating that the σ*$_{C–Cl}$ and π*$_{C=O}$ MOs are nearly identical in the transition state's LUMO. The energy level of orbital 22 (σ*) of
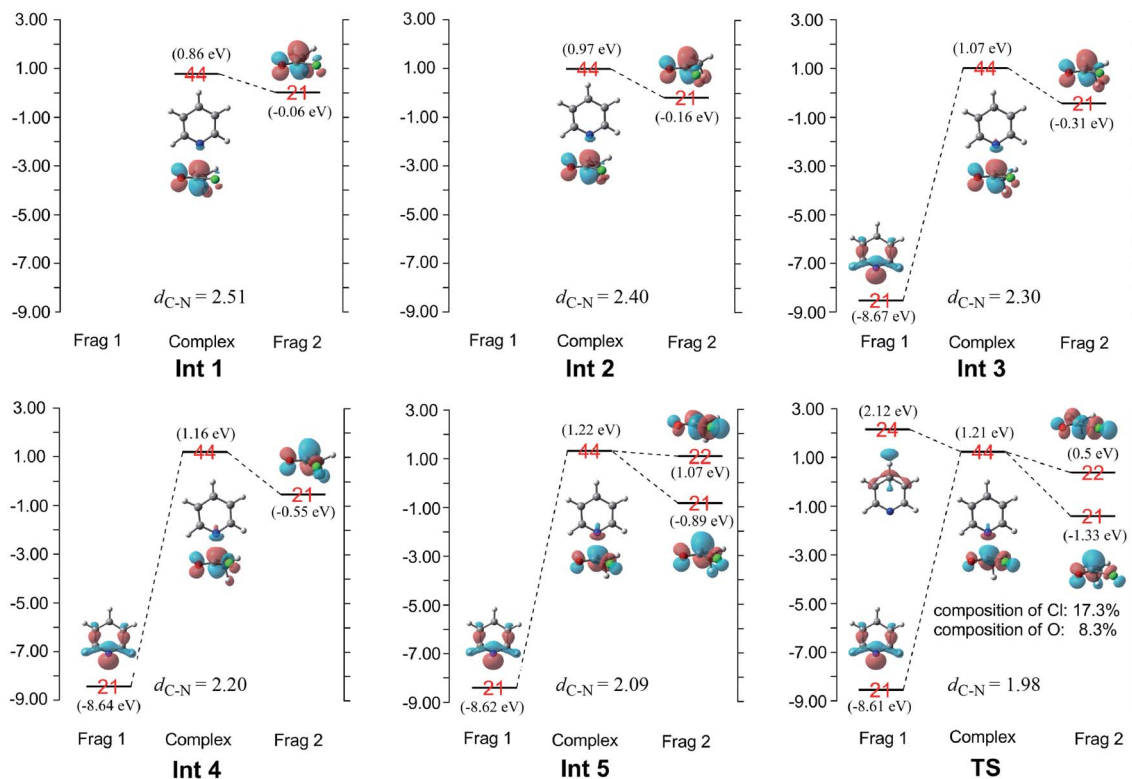
Fig. 4 Molecular orbital interaction diagrams of the intermediates and transition states implicated in the reaction of pyridine and acyl chloride (isosurface = 0.05 a.u.). The diagrams are constructed using fragments of pyridine (Frag 1) and acyl chloride (Frag 2).
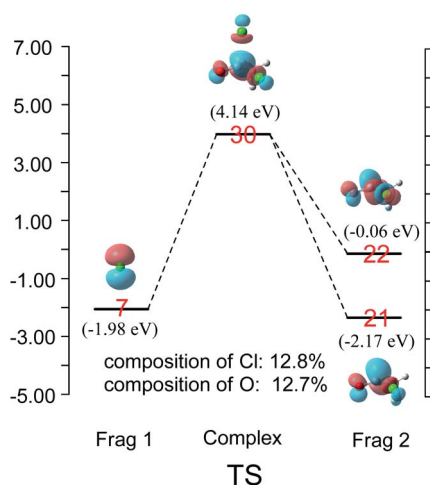

Fig. 5 Schematic molecular orbital interaction diagram showing the transition state of the reaction of Cl⁻ and acyl chloride (isosurface = 0.05 a.u.). Frag 1 and Frag 2 are fragments of Cl⁻ and acyl chloride, respectively.

CH_3COCl in TS_{Cl} reduced by 0.89 eV from free CH_3COCl, which is larger than that in $TS_{pyridine}$ (0.25 eV). Therefore, more $\pi^*_{C=O}$ MO mix into orbital 22 in TS_{Cl} compared to $TS_{pyridine}$ (as shown in Fig. 3 and 4). As a result, $\pi^*_{C=O}$ MO remains comparable contributions to σ^*_{C-Cl} in the transition state. This reaction mode is different from that observed in earlier studies, wherein
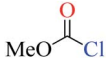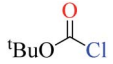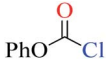
the σ^*_{C-Cl} MO was shown to be the main component of the LUMO of the transition state in the reaction of X^- (X = Cl, F) with CH_3COCl.[17–21]

An alternative mechanism of the nucleophilic substitution of CH_3COCl with pyridine is the in-plane σ attack with inversion ($S_N\sigma$-pyridine, Fig. 2).[15,16,21] The free energy barrier of this reaction is 29.5 kcal mol⁻¹ in dichloromethane, which is much higher than that of the S_Nm path (13.8 kcal mol⁻¹). The C–N and C–Cl bonds lengths in the $S_N\sigma$ transition state are 2.51 and 2.91 Å, respectively. Both bonds are longer than those observed in the S_Nm transition state, resulting in a larger free energy barrier of the $S_N\sigma$ reaction. However, the C–Cl bond lengths of the S_Nm and $S_N\sigma$ transition states corresponding to the reaction of CH_3COCl with Cl⁻ are 2.18 and 2.90 Å, respectively. The smaller difference between these two values compared to that determined for the reaction of CH_3COCl and pyridine indicates that the deformation energies of the two mechanisms (S_Nm and $S_N\sigma$) are close. Therefore, the related free energy barriers of the S_Nm and $S_N\sigma$ pathways of CH_3COCl + Cl⁻ are close (16.1 and 20.1 kcal mol⁻¹, respectively).

Chloroformates were also assessed. The energy values listed in Table 1 indicate that the reactions of these substrates (s2–s6; Scheme 2) with pyridine are similar to that of s1. Overall, the calculated energies suggested that the investigated chloroformates can easy react with pyridine under very low reaction temperature, which is consistent with previous experimental observations (−20 °C).[24,25] The very small energy gaps between the $\pi^*_{C=O}$ and σ^*_{C-Cl} MOs of all substrates (0.3 to 0.9 eV)

Table 1 Free energy barriers of the bimolecular nucleophilic substitution (S$_N$2) reactions of chloroformates with pyridine (kcal mol^{-1}), and the energy gaps between σ^*_{C-Cl} and $\pi^*_{C=O}$ of all substrates (eV)

	s2	s3	s4	s5	s6
	MeO—C(=O)—Cl	EtO—C(=O)—Cl	^{t}BuO—C(=O)—Cl	PhO—C(=O)—Cl	PhH$_2$CO—C(=O)—Cl
$\Delta G^{\neq}$	15.4	15.8	16.8	13.4	15.1
Energy gap	0.8	0.6	0.3	0.9	0.7

indicates that these MOs are efficiently mixed in the transition states.[17–19] Moreover, the main component of the LUMO of each transition state is the σ^*_{C-Cl} MO of the chloroformates. The optimized geometries of the transition states and the structures of the mixed orbitals are presented in Fig. S2–S3 of ESI.†

The transition state of the reaction of acyl bromide with pyridine (Fig. 6(a)) is similar to that of the acyl chloride. However, when the leaving group is F$^-$, no transition state is formed. Instead, the reaction of acyl fluoride with pyridine leads to a tetrahedral intermediate (Fig. 6(b)) that lies at 3.4 kcal mol^{-1} above the reactants (M06-2X level). The absence of a transition state for this reaction may be attributed to the greater strength of the C–F bond compared to the C–Cl bond.[19] A tetrahedron intermediate is also detected for the reaction of acyl fluoride with NH$_3$ (Fig. 6(c)). Based on M06-2X calculations, this intermediate lies at 5.4 kcal mol^{-1} above the reactants. The tetrahedral structure of the intermediate was verified using other theoretical methods including QCISD, MP2, PBE1PBE, B3LYP, B3LYP-d3, ωb97xd. The structures of these tetrahedral structures are illustrated in Fig. S1 in the ESI.† As for the reaction of CH$_3$COF with Cl$^-$, it shows only a product complex (CH$_3$COCl…F$^-$), with no transition state or tetrahedral intermediate. The CH$_3$COCl…F$^-$ complex is similar to that reported previously by Yamabe et al. for the reaction of CH$_3$COF with Cl$^-$.[17,18]

Fig. S4 in ESI† depicts the potential energy diagrams representing the reaction of acyl fluoride with different nucleophiles (pyridine, NH$_3$, and Cl$^-$). These diagrams clearly show stable intermediates for the reactions of acyl fluoride with pyridine

and NH$_3$, but not with Cl$^-$. According to previous studies, the formation of tetrahedron intermediate in nucleophilic substitution reactions of acyl chlorides is controlled by the leaving ability of the nucleofuge and by the energy gap between the $\pi^*_{C=O}$ and σ^*_{C-Cl} MOs.[18–20] In the case of acyl fluoride, the energy of newly formed bond in the product is also related to the formation of an intermediate. Based on our calculations, the bond energies of the newly formed C–N (pyridine), C–N (NH$_3$), and C–Cl in the products of the reactions of acyl fluoride with pyridine, NH$_3$, and Cl$^-$ are 79.1, 67.7 and 65.5 kcal mol^{-1}, respectively. With the least strong bond, the CH$_3$COCl…F$^-$ adduct is the least stable, and so, its formation is not favored. The greater strength of the C–N bond compared to the C–Cl bond also explains why the reaction barrier of nucleophilic substitution of CH$_3$COCl with pyridine is lower than that of substitution with Cl$^-$.

2 Nucleophilic substitution reactions of CH$_3$ClC=NOTf with pyridine or Cl$^-$

Pyridine may also be used as a nucleophile in substitution reactions of imidoyl substrates (C=N moiety, Scheme 2).[24,25] Based on our theoretical analyses, the nucleophilic substitution

Fig. 7 The nucleophilic substitution reactions of CH$_3$ClC=NOTf (s7) with pyridine or Cl$^-$. Reaction of pyridine with CH$_3$ClC=NOTf by (a) S$_N$m and (b) S$_N\sigma$ mechanisms, and reaction of Cl$^-$ with CH$_3$ClC=NOTf by (c) S$_N$m and (d) S$_N\sigma$ mechanisms.
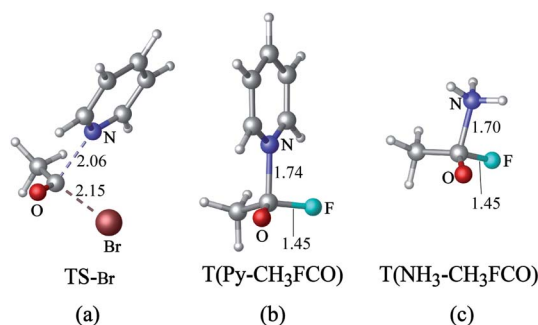

Fig. 6 (a) Transition state of the nucleophilic substitution reaction of acyl bromide with pyridine. Tetrahedron intermediates formed by reacting acyl fluoride with (b) pyridine and (c) NH$_3$.
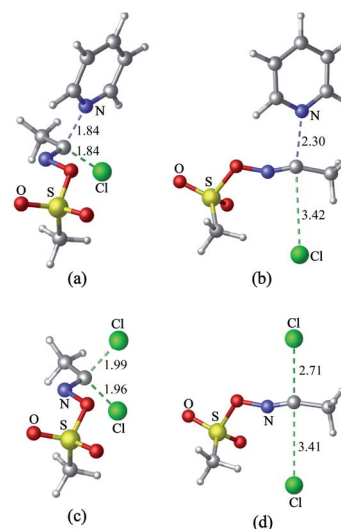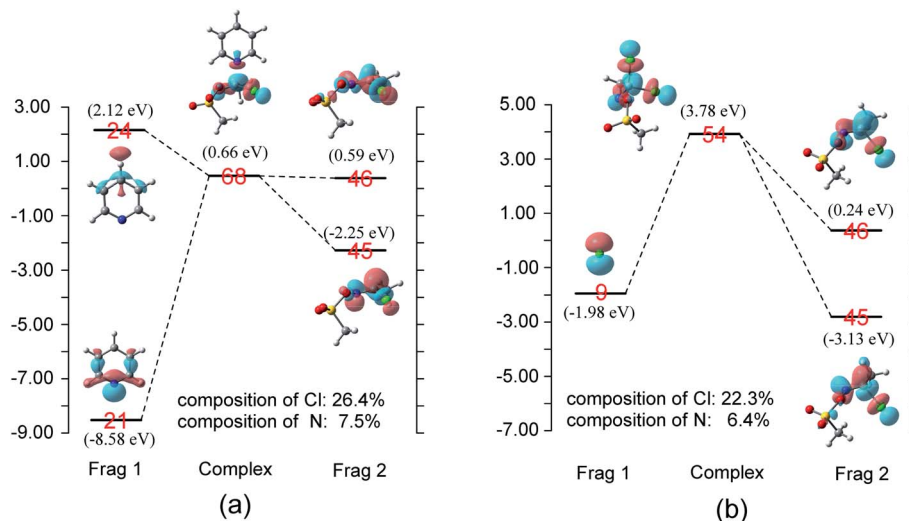
Fig. 8 Molecular orbital interaction diagrams showing the transition states of the reaction of (a) pyridine with $CH_3ClC=NOTf$, (b) Cl^- with $CH_3ClC=NOTf$ (isosurface = 0.05 a.u.). The diagrams are constructed using fragments of the pyridine or Cl^- (Frag 1) and $CH_3ClC=NOTf$ (Frag 2).

reaction of $CH_3ClC=NOTf$ (s7) with pyridine proceed *via* two possible mechanisms, S_Nm and $S_N\sigma$ (Fig. 7(a) and (b)), which are characterized by free energy barriers of 22.8 and 49.3 kcal mol^{-1}, respectively. The energy values indicate that the S_Nm pathway is relatively feasible, but the $S_N\sigma$ pathway is improbable under moderate reaction conditions. We recalculate the S_Nm reactions of substrate s7 using the ωb97xd and B3LYP-*d3* functionals. Related reaction barriers of S_Nm mechanism are 23.4 and 24.6 kcal mol^{-1}, respectively, in agreement with the values obtained using the M062X functional. The structures of transition states calculated by ωb97xd and B3LYP-*d3* functionals are shown in Fig. S1 in the SI.† As for reaction of $CH_3ClC=NOTf$ with Cl^-, it may occur *via* S_Nm and $S_N\sigma$ mechanisms (Fig. 7(c) and (d)), with free energy barriers of 26.5 and 40.0 kcal mol^{-1}, respectively. Overall, the calculated energy values suggest that the nucleophilic substitution of $CH_3ClC=NOTf$ (s7) with pyridine is more facile than that of Cl^-.

The energy gap between the $\pi^*_{C=N}$ and σ^*_{C-Cl} MOs of $CH_3ClC=NOTf$ is only 1.1 eV. Therefore, electron migration induces sufficient mixing of these two orbitals when pyridine reacts with $CH_3ClC=NOTf$. The CDA presented in Fig. 8(a) shows that the LUMO (orbital 68) of the transition state consists of mixed np (orbital 21, pyridine), orbitals 45 and 46 of $CH_3ClC=NOTf$, with σ^* orbital being the main component because of the large composition of chloride (26.4%). For the

reaction of Cl^- with $CH_3ClC=NOTf$, the CDA results of the transition state are similar to that observed in the reaction of pyridine with $CH_3ClC=NOTf$ (Fig. 8(b)). These reaction modes are similar to that observed in earlier studies.[17–21]

The reactions of the imidoyl substrates **s8–s13** with pyridine are similar to that of $CH_3ClC=NOTf$ (**s7**). As shown in Table 2, these reactions exhibit free energy barriers in the narrow range of 23.4–26.3 kcal mol^{-1}, which is higher than the energy barriers corresponding to the reaction of acyl chloride with pyridine. The free energy barriers of these reactions indicate that these reactions can occur under the condition of proper heating. In experiments, these reactions were carried out at 80 °C. Therefore, theoretical calculation results are reliable. Moreover, considering that the energy gaps between $\pi^*_{C=N}$ and σ^*_{C-Cl} MOs of the imidoyl substrates are low (0.5 and 2.4 eV), it may be concluded that these orbitals are efficiently mixed. Like $CH_3ClC=NOTf$, the main component of the transition state LUMOs of substrates (**s8–s13**) is the σ^*_{C-Cl} MO. The transition state and mixing orbitals of the imidoyl substrates are shown in Fig. S5 and S6 of ESI.†

The relationship between the free energy barrier and the product yield of the substrate (**s7–s11**) reaction with pyridine is shown in Fig. 9. As can be seen from Fig. 9, there is a good linear relationship between the yields of these reactions and the free energy barriers. The lower the free energy barrier, the higher the

Table 2 Free energy barriers of the bimolecular nucleophilic substitution (S_N2) reactions of chloro-oxime reagents with pyridine (kcal mol^{-1}). The energy gaps between σ^*_{C-Cl} and $\pi^*_{C=N}$ MOs of all substrates (eV)

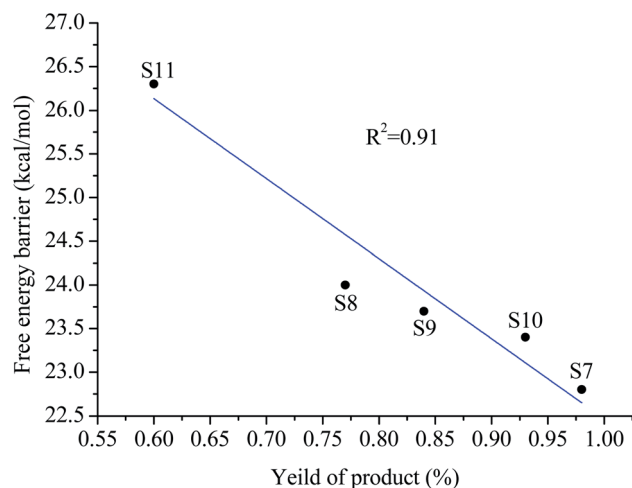|	s8	s9	s10	s11	s12	s13
	iPr $\overset{Cl}{\underset{N}{\diagup}}$ OMs	Ph $\overset{Cl}{\underset{N}{\diagup}}$ OMs	$(p\text{-}NO_2)Ph$ $\overset{Cl}{\underset{N}{\diagup}}$ OMs	$(o\text{-}NO_2)Ph$ $\overset{Cl}{\underset{N}{\diagup}}$ OMs	$(p\text{-}CH_3)Ph$ $\overset{Cl}{\underset{N}{\diagup}}$ OMs	$(p\text{-}CF_3)Ph$ $\overset{Cl}{\underset{N}{\diagup}}$ OM
$\Delta G^{\neq}$	24.0	23.7	23.4	26.3	23.6	23.9
Energy gap	0.5	1.7	1.1	2.2	2.2	2.4

Fig. 9 The relationship between the free energy barrier and the product yield of the substrate (s7–s11) reaction with pyridine.

yields. The theoretical calculation results are in good agreement with experimental observations. Thus, theoretical calculation results are reliable.

The reaction of $CH_3FC=NOTf$ with pyridine leads to the formation of a tetrahedral intermediate (Fig. 10, 19.9 kcal mol^{-1} above the reactants at the M06-2X level), which is characterized by C–N and C–F bond lengths of 1.61 and 1.42 Å, respectively. When Cl$^-$ is used as nucleophile, no stable adduct or transition state are evident, just like in the case of the reaction between Cl$^-$ and CH_3COF. The profile scans of nucleophile approach to $CH_3FC=NOTf$ (Fig. S7 in ESI†) confirm that a tetrahedral intermediate is formed with pyridine but not with Cl$^-$.

In summary, the reaction of pyridine with $CH_3XC=NOTf$ proceeds *via* a transition state when X is Cl$^-$ or forms a stable adduct when X is F$^-$. Similarly, a transition state is discerned for the substitution of $CH_3ClC=NOTf$ with Cl$^-$; however, the
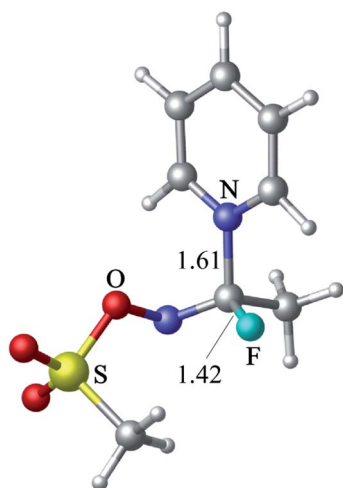

Fig. 10 Tetrahedral intermediate formed by reacting pyridine with $CH_3FC=NOTf$.
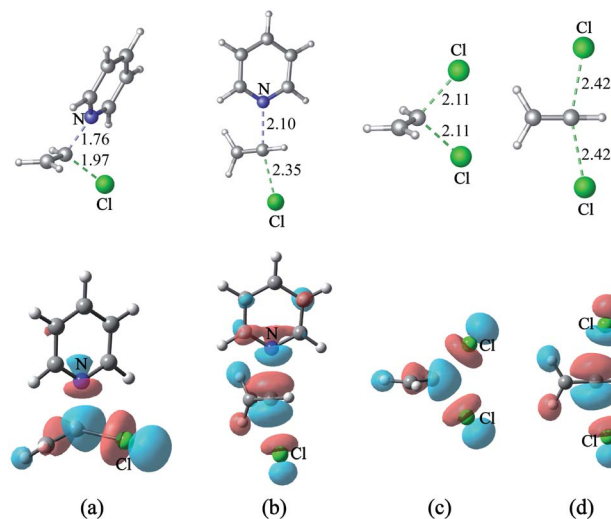

Fig. 11 The geometries and LUMO of transition states in the nucleophilic substitution reactions of $H_2C=CHCl$ with pyridine or Cl$^-$. Reaction of pyridine with $H_2C=CHCl$ by (a) S_NV-σv and (b) S_NV-σb mechanisms, and reaction of Cl$^-$ with $H_2C=CHCl$ by (c) S_NV-σv and (d) S_NV-σb mechanisms.

$CH_3FC=NOTf$ substrate shows neither a transition state nor a stable adduct when reacting with chloride.

3   Nucleophilic substitution reactions of $H_2C=CHCl$ with pyridine or Cl$^-$

The energy gap between the $\pi^*_{C=C}$ and σ^*_{C-Cl} molecular orbitals of $H_2C=CHCl$ (**s14**) is only 0.6 eV, so electron migration from pyridine or Cl$^-$ induces sufficient mixing of these two MOs. As shown in Fig. 11(a) – 10(d), the main components of each transition state's LUMO of the nucleophilic substitution reaction of $H_2C=CHCl$ with pyridine or Cl$^-$ is the σ^*_{C-Cl} MO of $H_2C=CHCl$. The mechanism is different from earlier studies, wherein the S_NV reactions proceed *via* concerted π attack ($S_NV\pi$) or *via* in-plane σ^* attack ($S_NV\sigma$).[11–14] There are two ways nucleophile attack $H_2C=CHCl$. One way is for nucleophile to attack the reactive molecule vertically (the mode is labeled S_NV-σv, Fig. 10(a) and (c)), and the other way is to attack it from backside (the mode is labeled S_NV-σb, Fig. 11(b) and (d)).

The free energy barriers of the reaction of pyridine with $H_2C=CHCl$ (**s14**) *via* the S_NV-σv and S_NV-σb mechanisms are 42.4 and 47.5 kcal mol^{-1}, respectively. Similarly, the related free energy barriers for the reaction of $H_2C=CHCl$ with Cl$^-$ *via* two modes are 47.9 kcal mol^{-1} and 42.3 kcal mol^{-1}, respectively. The calculated barriers are consistent with that reported by the group of Radom.[48] It can be concluded that S_NV-σv is more facile than S_NV-σb. $CH_3HC=CCH_3Cl$ (**s15**) and $Cl_2C=CCl_2$ (**s16**) are also tested as substrates, and the free energy barriers of their nucleophilic substitution reactions with pyridine are 46.0 and 38.2 kcal mol^{-1}, respectively (S_NV-σv mode).

Conclusion

The mechanisms of nucleophilic substitution of carbonyl, imidoyl, and vinyl carbon centers with pyridine or halides are

investigated using detailed density functional theory calculations. The main conclusions are summarized below.

(1) The transition state LUMOs of the reactions of RCOCl with pyridine, RClCNR with pyridine and RClCNR with Cl$^-$ are composed of mixed orbitals (part from pyridine or Cl$^-$ and part from substrate), with the σ^* MO of the substrate being the main component. However, for the reaction of Cl$^-$ and CH$_3$COCl, the σ^*_{C-Cl} and $\pi^*_{C=O}$ MOs are nearly identical in the transition state's LUMO. This type of transition state has not been reported previously for nucleophilic substitution reactions of acyl chlorides. In fact, earlier studies show that the transition state LUMOs corresponding to the reaction of CH$_3$COCl with halides are composed primarily of the σ^*_{C-Cl} MO. The newly discovered reaction mode is called S$_N$m (m means mix).

(2) For the reactions of H$_2$C=CHCl with pyridine and Cl$^-$, the main components of each transition state's LUMO is the σ^*_{C-Cl} MO. The mechanism is different from earlier studies, wherein the S$_N$V reactions proceed *via* concerted π attack (S$_N$Vπ) or *via* in-plane σ^* attack (S$_N$Vσ). According to the way of attack, there are two ways nucleophile attack H$_2$C=CHCl (S$_N$V-σv and S$_N$V-σb).

(3) The reactions of pyridine with RCOX and RXCNR proceed *via* transition states when X is Cl$^-$; however, when X is F$^-$, a tetrahedral intermediate is formed instead. Similarly, transition states are observed for the reactions of RCOCl and RClCNR with Cl$^-$, but no transition states or intermediate are detected for the RCOF and RFCNR substrates. Our results suggest that adduct formation is favored by stronger C–X bonds (X = pyridine, NH$_3$, or Cl$^-$).

S$_N$V reactions are involved in several biological processes, and we believe that our proposed mechanism can provide inspiration for the study of these biological processes. In the future, we would like to investigate other neutral nucleophiles so as to discover new bimolecular nucleophilic substitution reactions.

Conflicts of interest

There are no conflicts to declare.

Acknowledgements

Notes and references

1 W. L. Hase, *Science*, 1994, **266**, 998–1002.
2 M. L. Chabinyc, S. L. Craig, C. K. Regan and J. I. Brauman, *Science*, 1998, **279**, 1882–1886.
3 J. Mikosch, S. Trippel, C. Eichhorn, R. Otto, U. Lourderaj, J. X. Zhang, W. L. Hase, M. Weidemüller and R. Wester, *Science*, 2008, **319**, 183–186.
4 I. Szabó and G. Czakó, *Nat. Commun.*, 2015, **6**, 5972–5977.
5 J. Xie, R. Otto, J. Mikosch, J. Zhang, R. Wester and W. L. Hase, *Acc. Chem. Res.*, 2014, **47**, 2960–2969.
6 J. Xie and W. L. Hase, *Science*, 2016, **352**, 32–33.
7 T. A. Hamlin, M. Swart and F. M. Bickelhaupt, *ChemPhysChem*, 2018, **19**, 1315–1330.
8 Y. G. Proenza, M. A. F. de Souza and R. L. Longo, *Chem. – Eur. J.*, 2016, **22**, 16220–16229.
9 T. A. Hamlin, B. van Beek, L. P. Wolters and F. M. Bickelhaupt, *Chem. – Eur. J.*, 2018, **24**, 5927–5938.
10 J. Z. A. Laloo, L. Rhyman, O. Larrañaga, P. Ramasami, F. M. Bickelhaupt and A. de Cózar, *Chem.–Asian J.*, 2018, **13**, 1138–1147.
11 V. Lucchini, G. Modena and L. Pasquato, *J. Am. Chem. Soc.*, 1995, **117**, 2297–2300.
12 C. K. Kim, K. H. Hyun, C. K. Kim and I. Lee, *J. Am. Chem. Soc.*, 2000, **122**, 2294–2299.
13 C. F. Bernasconi and Z. Rappoport, *Acc. Chem. Res.*, 2009, **42**, 993–1003.
14 I. Fernández, F. M. Bickelhaupt and E. Uggerud, *J. Org. Chem.*, 2013, **78**, 8574–8584.
15 H. G. Li, C. K. Kim, B. Lee, C. K. Kim, S. K. Rhee and I. Lee, *J. Am. Chem. Soc.*, 2001, **123**, 2326–2333.
16 J. M. Fox, O. Dmitrenko, L. Liao and R. D. Bach, *J. Org. Chem.*, 2004, **69**, 7317–7328.
17 S. Yamabe and T. Minato, *J. Org. Chem.*, 1983, **48**, 2972–2975.
18 S. Yamabe, T. Minato and Y. Kawabata, *Can. J. Chem.*, 1984, **62**, 235–240.
19 I. Lee, D. Lee and C. K. Kim, *J. Phys. Chem. A*, 1997, **101**, 879–885.
20 I. Lee, C. K. Kim, H. G. Li, C. K. Sohn, C. K. Kim, H. W. Lee and B.-S. Lee, *J. Am. Chem. Soc.*, 2000, **122**, 11162–11172.
21 C. K. Kim, H. G. Li, H. W. Lee, C. K. Sohn, Y. I. Chun and I. Lee, *J. Phys. Chem. A*, 2000, **104**, 4069–4076.
22 D. D. Sung, T. J. Kim and I. Lee, *J. Phys. Chem. A*, 2009, **113**, 7073–7079.
23 I. S. Han, C. K. Kim, C. K. Sohn, E. K. Ma, H. W. Lee and C. K. Kim, *J. Phys. Chem. A*, 2011, **115**, 1364–1370.
24 J. A. Bull, J. J. Mousseau, G. Pelletier and A. B. Charette, *Chem. Rev.*, 2012, **112**, 2642–2713.
25 P. S. Fier, *J. Am. Chem. Soc.*, 2017, **139**, 9499–9502.
26 M. J. Frisch; G. W. Trucks; H. B. Schlegel; G. E. Scuseria; M. A. Robb; J. R. Cheeseman; G. Scalmani; V. Barone; B. Mennucci; G. A. Petersson; H. Nakatsuji; M. Caricato; X. Li; H. P. Hratchian; A. F. Izmaylov; J. Bloino; G. Zheng; J. L. Sonnenberg; M. Hada; M. Ehara; K. Toyota; R. Fukuda; J. Hasegawa; M. Ishida; T. Nakajima; Y. Honda; O. Kitao; H. Nakai; T. Vreven; J. A. Montgomery Jr.; J. E. Peralta; F. Ogliaro; M. Bearpark; J. J. Heyd; E. Brothers; K. N. Kudin; V. N. Staroverov; R. Kobayashi; J. Normand; K. Raghavachari; A. Rendell; J. C. Burant; S. S. Iyengar; J. Tomasi; M. Cossi; N. Rega; J. M. Millam; M. Klene; J. E. Knox; J. B. Cross; V. Bakken; C. Adamo; J. Jaramillo; R. Gomperts; R. E. Stratmann; O. Yazyev; A. J. Austin; R. Cammi; C. Pomelli; J. W. Ochterski; R. L. Martin; K. Morokuma; V. G. Zakrzewski; G. A. Voth; P. Salvador; J. J. Dannenberg; S. Dapprich; A. D. Daniels; O. Farkas; J. B. Foresman; J. V. Ortiz; J. Cioslowski and D. J. Fox *Gaussian 16, Revision A.03*, Gaussian, Inc., Wallingford, CT, 2016.

27 Y. Zhao and D. G. Truhlar, *Theor. Chem. Acc.*, 2008, **120**, 215–241.

28 Y. Zhao and D. G. Truhlar, *Acc. Chem. Res.*, 2008, **41**, 157–167.

29 J. Miao, S. Hua and S. Li, *Chem. Phys. Lett.*, 2012, **541**, 7–11.

30 R. Krishnan, J. S. Binkley, R. Seeger and J. A. Pople, *J. Chem. Phys.*, 1980, **72**, 650–654.

31 J. Tomasi, B. Mennucci and R. Cammi, *Chem. Rev.*, 2005, **105**, 2999–3094.

32 K. Fukui, *Acc. Chem. Res.*, 1981, **14**, 363–368.

33 H.-P. Hratchian and H.-B. Schlegel, *Theory and Applications of Computational Chemistry: The First 40 Years*, ed. C. E. Dykstra, Elsevier, Amsterdam, 2005, pp. 195–249.

34 K.-B. Wiberg, *Tetrahedron*, 1968, **24**, 1083–1096.

35 A.-E. Reed, L.-A. Curtiss and F. Weinhold, *Chem. Rev.*, 1988, **88**, 899–926.

36 F. Weinhold, *J. Comput. Chem.*, 2012, **33**, 2363–2379.

37 C.-Y. Legault, *CYLview, 1.0b*, Université de Sherbrooke, 2009, http://www.cylview.org.

38 S. Dapprich and G. Frenking, *J. Phys. Chem.*, 1995, **99**, 9352–9362.

39 W. Li, L. Chen, Z. Lin, S. Man, X. Qin, Y. Lyu, C. Li and G. Leng, *Inorg. Chem.*, 2020, **59**(14), 9667–9682.

40 Y. Yang, X. Hou, T. Zhang, J. Ma, W. Zhang, S. Tang, H. Sun and J. Zhang, *J. Org. Chem.*, 2018, **83**(19), 11905–11916.

41 L. Liu, B. Sun, R. Ding and Y. Mao, *J. Phys. Chem. A*, 2020, **124**(52), 11093–11101.

42 L. M. Loftus, A. Li, K. L. Fillman, P. D. Martin, J. J. Kodanko and C. Turro, *J. Am. Chem. Soc.*, 2017, **139**(50), 18295–18306.

43 F. L. Hirshfeld, *Theor. Chim. Acta*, 1977, **44**, 129–138.

44 P. Bultinck, C. V. Alsenoy, P. W. Ayers and R. Carbó-Dorca, *J. Chem. Phys.*, 2007, **126**, 144111.

45 T. Lu and F. Chen, *J. Comput. Chem.*, 2012, **33**, 580–592.

46 T. Lu and F. Chen, *J. Mol. Graphics Modell.*, 2012, **38**, 314–323.

47 G. Knizia and J. E. M. N. Klein, *Angew. Chem., Int. Ed.*, 2015, **54**, 5518–5522.

48 M. N. Glukhovtsev, A. Pross and L. Radom, *J. Am. Chem. Soc.*, 1994, **116**, 5961–5962.